Article

Impact of Wire Selection on the Performance of an Induction Motor for Automotive Applications

Lino Di Leonardo * , Giuseppe Fabri , Andrea Credo , Marco Tursini and Marco Villani

Department of Industrial and Information Engineering and Economics, University of L'Aquila,
67100 L'Aquila, Italy; giuseppe.fabri@univaq.it (G.F.); andrea.credo@univaq.it (A.C.);
marco.tursini@univaq.it (M.T.); marco.villani@univaq.it (M.V.)
* Correspondence: lino.dileonardo@univaq.it

Abstract: This paper investigates the impact of the wire selection on the performance of induction motors for automotive applications. The section of wire and the material are evaluated at a high speed of 200 kW in an induction motor designed for premium vehicle applications. The proposed solutions have the same electromagnetic and thermal constraints, as well as the same final encumbrance. The various wire and winding types differ in terms of slot design, phase resistance, end-winding overhanging portion, skin and proximity effects, and equivalent slot thermal conductivity. Their impacts are analyzed in terms of the operating area motor efficiency and they are tested in an automotive drive cycle, highlighting the advantages and disadvantages of each configuration.

1. Introduction

In recent years there has been a growing interest in hairpin motors thanks to their use in innovative and especially prominent fields, such as in the automotive industry, where they enhance the performance of the drivetrain, for example by enhancing the power density.

Hairpins are conductors with a solid and rectangular cross-section, as opposed to the stranded wire ones utilized traditionally. Thanks to their higher slot fill factor (more than 0.75), better thermal slot propagation is ensured, meaning higher torque and power density values are possible when compared to classical round conductors [1–10].

Moreover, hairpin windings have the benefit of enabling a highly automated production processes, allowing for high-quality stator manufacturing at low cost for mass production. In particular, the production process involves inserting the pre-folded hairpin in the rectangular slot axially (welding the adjacent winding sections) or radially (having a unique winding section and avoiding the welding but requiring an open stator slot) [11].

Nevertheless, the hairpins' large cross-section is affected by skin and proximity effects [12,13], with consequent nonuniform current distribution and losses. The effects increase when the motor is fed by an inverter [14], whereby the PWM modulation introduces high current harmonics, which are meaningful at the high fundamental frequencies demanded for high-speed operation of the machine [15].

The classical techniques suggest reducing skin and proximity effects by increasing the number of conductors in the slot, and if necessary by using parallel paths and conductor transposition if possible [16]. Other techniques are proposed in the literature to reduce these effects, such as the use of variable cross-section flat wires, an increased parallel path when close to the airgap, and the placement of the conductors far from the airgap [17].

All of these techniques share the common disadvantage of increasing the manufacturing complexity in terms of the time and cost, but may also lead to a lower slot fill factor

and higher DC copper loss. Therefore, the number of conductors within each slot is limited to 8 ÷ 10 by the actual manufacturing process, with a slot fill factor of up to 0.7 [18–20].

Another approach, in which both the scientific community and the automotive industry have shown interest, involves the use of aluminum hairpins instead of copper ones [21], a permanent magnet synchronous machine [22], and a segmental rotor-switched reluctance machine [23] This topic is not only of interest to motor winding designers, but aluminum has been adopted even in rotor cages [24], transformers [25], and transmission lines [26].

Recently, the price of copper increased by up to 50% from 2020 to 2021 [27], motivating plans to reduce the use of copper in the motor industry. Hence, aluminum hairpins have become particularly attractive due to their market availability and more stable costs (with twice the worldwide production rate of copper).

The evaluation of the most suitable winding material in the early design steps can reduce the costs of the machine, while high power density levels and lower losses can also be pursued.

Indeed, from an electrical point of view, aluminum has a lower conductivity rate than copper (Table 1). Since the skin depth is proportional to the square root of the resistivity, it is less affected by the eddy losses [28,29]. For instance, considering a frequency of 50 Hz and a temperature of 75 °C, the penetration depth of copper is 9.4 mm, while for aluminum it is 12.3 mm; therefore, the eddy losses in aluminum windings are 38% lower than in copper windings at the same volume of the conductor. Considering that eddy current losses increase with the harmonic order with the square of the frequency, this aspect becomes meaningful in the winding design for high-speed machines or in the presence of high-frequency current harmonics.

Table 1. Material properties of aluminum and copper.

	Unit	Aluminum	Copper
Electrical Properties			
Electrical resistivity (20 °C)	10–8 mΩ	2.6	1.7
Resistance heat exchange	1/°C	0.004	0.0039
Mechanical Properties			
Density	g/cm^3	2.7	8.92
Young's Modulus	GPa	70	120–140
Yield strength	MPa	11 (pure), 400 (alloys)	40–80
Ultimate Tensile Strength	MPa	90 (pure), 600 (alloys)	210
Hardness (Vickers)	MPa	167	350–390
Thermal Properties			
Melting Point	°C	660	1083
Boiling Point	°C	2467	2562
Thermal Conductivity	W/mK	235	400
Thermal Expansion Coefficient	μm/mK	23.1	16.5
Specific Heat	J/g K	0.9	0.38
Heat of Fusion	kJ/mol	10.79	13.05

Moreover, from a mechanical point of view, the low density of aluminum can reduce the weight of the windings, in addition to providing excellent flexibility, and can simplify the winding production processes. Additional promising qualities include the good malleability during the welding process and having a thermal expansion rate closer to that of potting resins at low temperatures [30].

The combination of these features can make aluminum hairpins attractive to many industries, in particular in the automotive industry, where the lower electrical and thermal conductivity rates with respect to copper may be balanced by the lower high-frequency losses in high-speed motors.

In particular, the adoption of aluminum in replacing copper requires an appropriate winding design to enhance the specific power and efficiency.

The aim of the article is to investigate the performance of a motor for automotive applications by changing the winding section and material. In particular, the reference motor is an induction motor (IM) developed within the framework of the Horizon 2020 ReFreeDrive project (Rare Earth Free e-Drives) [31,32]. The induction motor is a useful technology as it reduces rare-earth magnet use, making it an attractive and feasible solution in the automotive industry due to its simple manufacturing process, robustness, versatility, cost-effectiveness, and fault-tolerant capabilities [33].

Section 2 discusses general machine design rules for copper hairpins, copper-stranded wires, and aluminum hairpins. Sections 3 and 4 report on the electromagnetic and thermal performance of the proposed windings, respectively, at rated and peak power. In Section 5, the performances in the drive cycle are addressed, focusing on the efficiency aspects of the proposed winding technologies.

2. Proposed Designs for Investigation

To focus on the windings' impact on the performance, an investigation was carried out starting from a reference design of an electric motor for EV traction applications, already featuring copper hairpin windings (here labelled as design D1).

The 200 kW IM motor designed in the framework of the ReFreeDrive project [32] as a traction motor for premium vehicles was taken as the reference. The key performance indicators (KPIs) for the motor design, including the efficiency, specific torque, specific power, and power density, are reported in Table 2, while the main design choices and optimization process are described in [31,34].

Table 2. Motor requirements.

Requirement	Unit	Value
Peak power	kW	200
Peak torque	Nm	371
Maximum speed (target)	rpm	22,000
Nominal torque	Nm	152
Nominal power	kW	70
Peak specific power *	kW/Kg	4.3
Peak specific torque *	Nm/kg	8.2
Peak power density *	kW/L	8
Efficiency	%	$\geq$94
Maximum DC bus voltage	V	800
Maximum phase current	Arms	500
Maximum dimensions	mm	$250 \times 250 \times 310$

* Active material only.

A high rotational speed (22,000 rpm) was selected to increase the specific power of the machine, while a gear ration of 11.62 was envisioned for the target vehicle.

The machine design is outlined in Figure 1, where a 36-slot stator and 50-bar rotor are used in a 4-pole configuration, while a copper hairpin winding is used on the stator side. The proposed winding design is based on the proprietary manufacturing technology developed by Tecnomatic SpA, using precision-formed rectangular wires (4 conductors per slot) that comprise multiple layers of interlocking "hairpins", as shown in the figure, providing a high slot fill factor (up to 73%). For the stator and rotor laminations, a silicon–iron alloy (M235-35A fully processed, 0.35 mm thickness) was selected, which offers a good compromise between cost and performance. The rotor has a die-casted pure copper cage that guarantees higher mechanical robustness and better thermal properties, as well as improved conductivity with respect to aluminum cages. Due to the high rotor speed, the mechanical integrity of the rotor core and copper cage were verified. A detailed design analysis leading to the specific machine topology detailed in [34]. The main electromagnetic and geometrical data of the initial design are reported in Table 3.
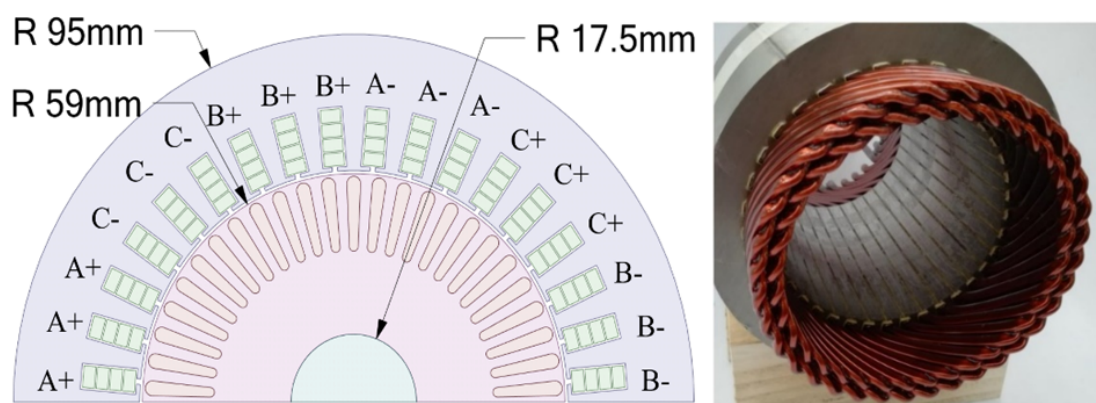
Figure 1. Main geometrical details of initial design D1 (**left**) and prototype view of the hairpin winding (**right**) (courtesy of Tecnomatic S.p.A.).

Table 3. Main design data for reference IM machine (design D1).

Design Data	Description	Value
p	Pole pairs	2
Q_s	Stator slots	36
Q_r	Number of rotor bars	50
n_L	Number of series conductors per slot	4
R_{os}	Outer stator radius	95 mm
R_{is}	Inner stator radius	59.8 mm
R_{or}	Outer rotor radius	59 mm
R_{ir}	Inner rotor radius	17.5 mm

The reference design D1 is equipped with a proper cooling system based on two main elements, a spiral stator water jacket and a spiral shaft groove, where the envisioned cooling fluid is a 50/50 water–ethylene glycol mixture.

The 4-pole, 36-slot, 50-bar topology of reference design D1 was refined to investigate the impacts on the performance of different motor windings, as follows:

- Stranded copper winding, round wire, leading to design D2;
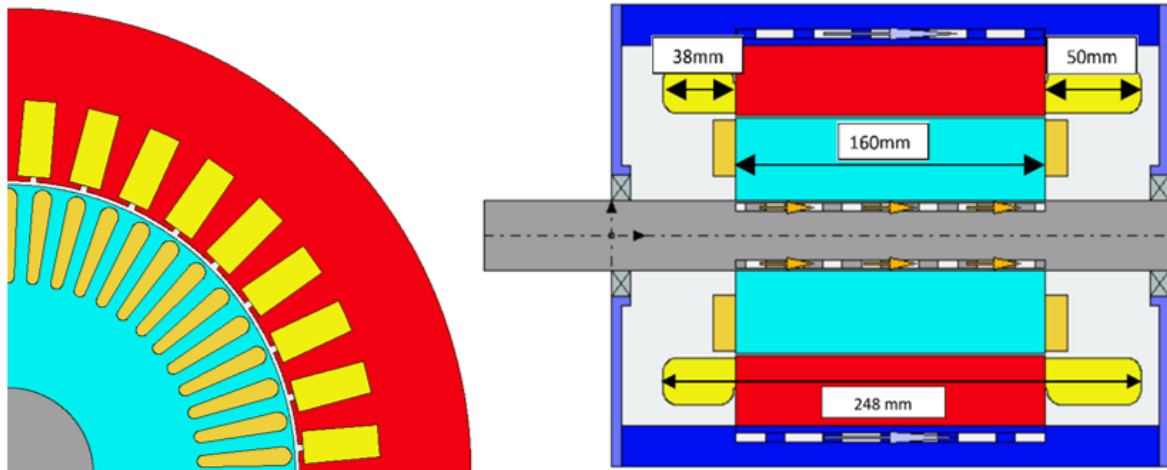- Aluminum hairpin winding, leading to design D3.

The aim of the machine refinements was to optimize the motor performance at the rated working point in terms of the efficiency and torque ripple, considering also the same encumbrance and thermal limits imposed by the insulation. The radial dimensions of the rotor are kept the same for all designs, since they are optimized from a mechanical point of view.

The refinements made to achieve design D2 involve a re-designed stator with a stranded winding with the same outer diameter. The new stator has a classical parallel tooth used for round-wire windings, with a size considering the rated current (192 A_{pk}) that permits the same maximum temperature at a steady state reached by design D1 (180 °C). A slot fill factor of 40% is envisioned to be achieved for automatic winding machines.

The third proposed design D3 also involves a re-designed stator with an aluminum hairpin winding with the same slot fill factor as the copper hairpin winding (73%). The new stator has a trapezoidal tooth, with the same typology used for D1 but re-sized for the new rated current (220 A_{pk}), permitting the same maximum insultation temperature at steady state as for D1.

The active stack length of each design was modified to comply with the maximum package envelope of 310 mm. The refinement of the stack length took into account the different end-winding overhanging portions envisioned for each winding technology.
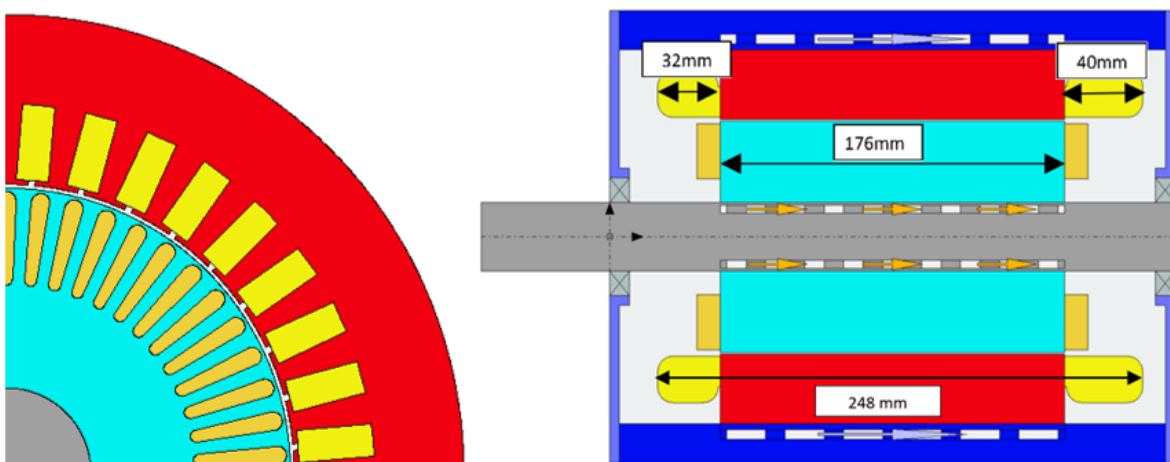
Figure 2 shows the radial and axial cross-sections of the initial design D1 with a copper hairpin, design D2 with a stranded copper winding, and design D3 with an aluminum hairpin winding.

Design D1: Copper hairpin (**a**)
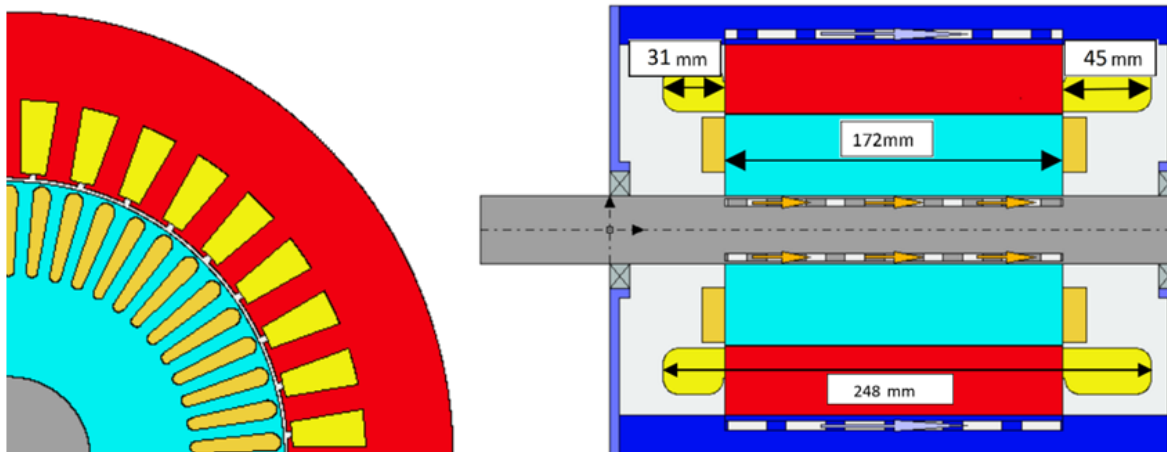
Design D2: Stranded copper winding (**b**)

Design D3: Aluminum hairpin (**c**)

Figure 2. Radial and axial cross-sections of the IM designs: (**a**) design D1; (**b**) design D2; (**c**) design D3.

The main axial geometrical data for the three compared designs are reported in Table 4 and shown in Figure 2.

Table 4. Comparison of the IM designs.

Parameter	Description	D1	D2	D3
L	Stack length	160 mm	172 mm	176 mm
FF	Slot fill factor	0.72	0.36	0.72
O_{is}	Overhang insertion side	38 mm	31 mm	32 mm
O_{ws}	Overhang welded side	50 mm	45 mm	40 mm
R_{DC}	Winding DC resistance	0.018 Ω	0.0326 Ω	0.028 Ω
I_{Rated}	Rated phase current	280 A_{pk}	192 A_{pk}	220 A_{pk}
W [1]	Motor weight	39.8 kg	38.1 kg	37.5 kg
$W_{windings}$	Stator windings weight	7.2 kg	3.3 kg	2.1 kg

[1] Including stator and rotor lamination, stator windings, rotor cage, and shaft.

The 4-pole, 36-slot, 50-bar topology appeared to be the recommended combination for all the three designs.

The aluminum hairpin winding has a smaller end-winding overhanging portion thanks to its better malleability compared with copper, meaning the simple bending and forming capabilities of this metal can be exploited whether it is hot or cold. This gives this technology added value, allowing it to mitigate the higher DC resistance of the aluminum by reducing the length of the winding and enlarging the stack length, improving the performance in terms of efficiency and thermal behavior.

Nevertheless, although the end-winding overhanging portion for the aluminum hairpin is inferior to the copper one, the DC resistance of design D3 is still greater than D1 due to the greater conductivity of the material (same slot fill factor in D1 and D3). However, when compared with design D2, where the stranded wire technology has a lower slot fill factor, the aluminum hairpin has better DC resistance. The different DC resistance levels are strictly linked to the definition of the rated current shown in Table 5, limited by the steady-state thermal behavior of the different configurations.

Table 5. Induction motors performances at rated operating points.

Description	D1	D2	D3
Speed	6000 rpm	6000 rpm	6000 rpm
Rated Phase Current	280 A (peak)	192 A (peak)	220 A (peak)
Phase Voltage	268 V (peak)	265 V (peak)	276 V (peak)
Frequency	202 Hz	201 Hz	202 Hz
Slip	0.0093	0.0067	0.0077
Torque	120 Nm	84 Nm	100 Nm
Output power	75 kW	51 kW	61 kW
Efficiency	93.5%	92.8%	93.3%

Furthermore, the density of the aluminum reduces the weight of the hairpin windings by 5.1 kg, achieving a 2.3 kg weight reduction at the machine level compared to the heavier copper hairpin winding machine. A minor weight reduction is achieved by replacing copper-stranded round wires with aluminum hairpins (1.2 kg at the winding level, 0.6 kg at the machine level)

For the purpose of a cost assessment, the weights of the stator windings are shown in the Table 4. Considering the weights of the active materials, the 2022 material costs, and a mass production rate of 100 k pieces/year, neglecting the slight stack length variation, the aluminum winding technology is estimated to achieve up to a 15% cost reduction compared to copper hairpin machines (with slightly lower performance) and a up to 5% cost reduction compared to copper-stranded wires (with better performance).

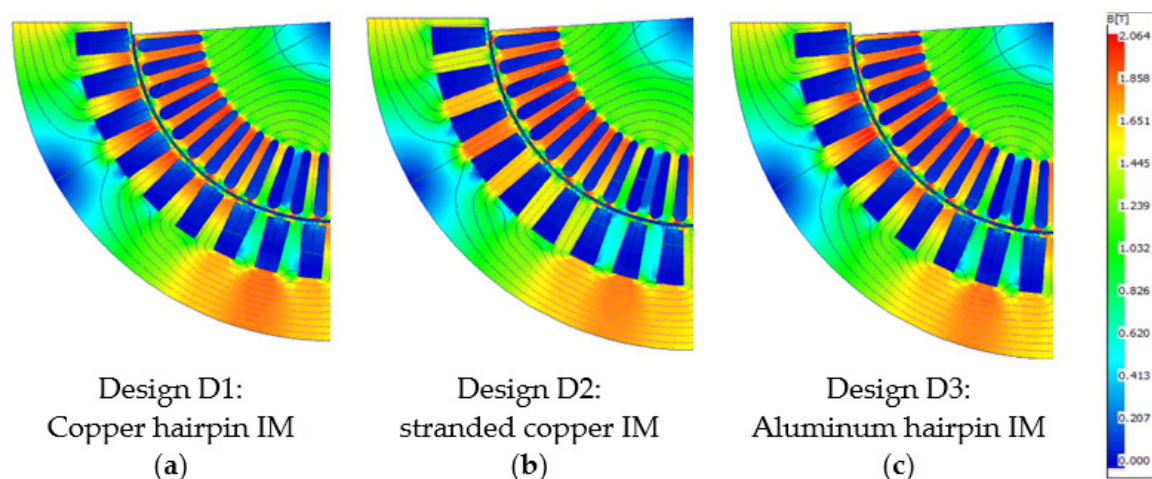## 3. Electromagnetic and Thermal Performance at Rater Power

Here, the performance of each design is detailed, whereby the rated operating point is set for all three designs at 6000 rpm as per the initial design specifics. As previously discussed, the rated current is evaluated for each design considering the continuous thermal limits. In particular, the proposed insulation is class H, with a maximum allowed temperature of 180 °C. The frequency and slip are modified to maximize the efficiency for each design. The performances of the proposed designs are listed in the following Table 6.

Table 6. Performances at the peak-power working point for the three proposed designs.

| Description	D1	D2	D3
Speed	6000 rpm	6000 rpm	6000 rpm
Phase current	707 A (peak)	707 A (peak)	707 A (peak)
Phase voltage	271 V (peak)	314 V (peak)	309 V (peak)
Frequency	205 Hz	204 Hz	204 Hz
Slip	0.0233	0.0205	0.0207
Torque	340 Nm	375 Nm	380 Nm
Output Power	209 kW	230 kW	233 kW
Efficiency	89.53	86.2	88.1

The rated current (and consequently the torque) for D1 can be higher due to the lower resistance value, also improving the efficiency and increasing the output power. Solution D2, on the other hand, has the lowest rated current, reducing the torque value by 30% and efficiency by 0.7% compared to D1. The third solution is placed in the middle of the other two, with a reduction in torque of 17.3% and a reduction in efficiency of 0.2% compared to D1.

The flux densities of the three proposed designs are reported in Figure 3 for verification that each design reaches a similar level of material saturation.
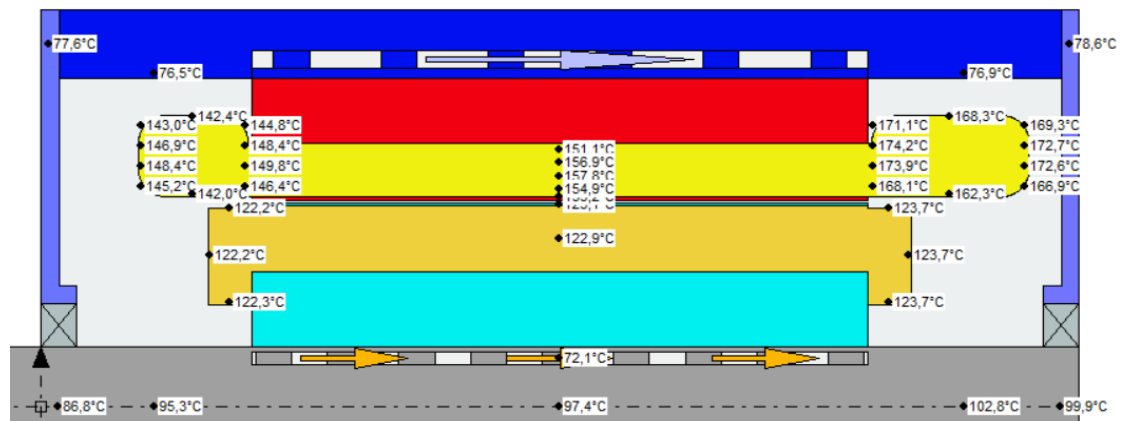

Design D1:
Copper hairpin IM
(a)

Design D2:
stranded copper IM
(b)

Design D3:
Aluminum hairpin IM
(c)

Figure 3. Flux density and flux isoline distribution: (**a**) design D1; (**b**) design D2; (**c**) design D3.

At the same time, the steady-state thermal analysis is carried out to evaluate the maximum temperature reached during continuous operation considering the different stack lengths, the higher thermal conductivity of copper compared to aluminum in the windings, and the consequent better ability to transport heat from the slot to the core. Figure 4 shows the temperatures for the three compared models starting from an ambient temperature of 50 °C and with the same cooling system.
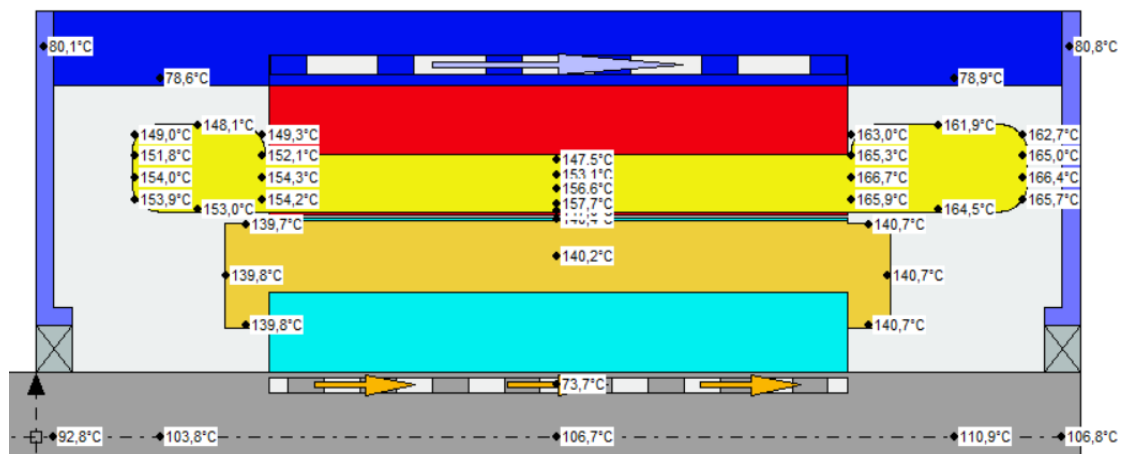
Design D1: Copper hairpin (**a**)

Design D2: Stranded winding (**b**)
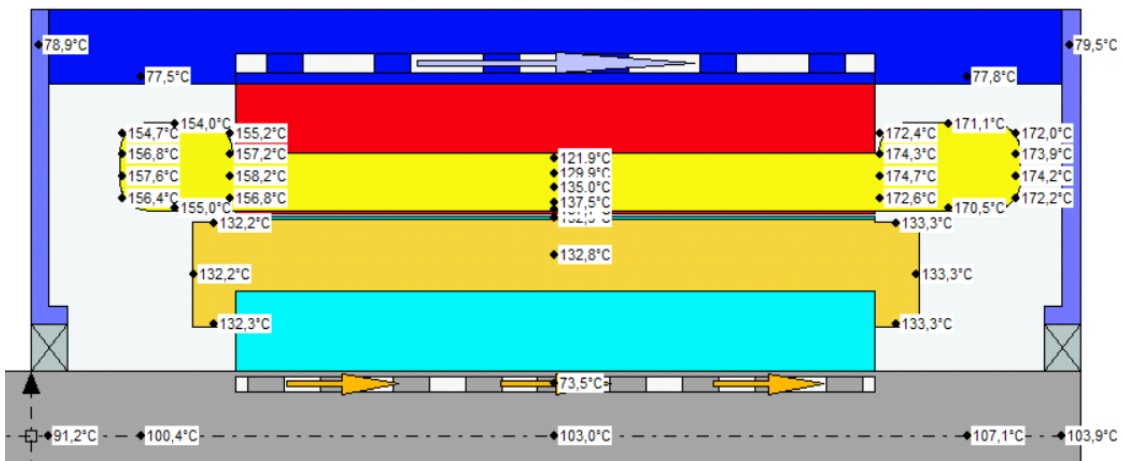
Design D3: Aluminum hairpin (**c**)

Figure 4. Steady-state temperature at rated power and ambient temperature of 50 °C for the same cooling system: (**a**) design D1; (**b**) design D2; (**c**) design D3.

As confirmed, the temperature hotspots for all the three proposed designs with the rated current reach a steady state just below the maximum temperature allowed for insulation class H. The same temperature limit will also be fixed in the next section to evaluate the peak power performance.

4. Electromagnetic and Thermal Performance at Maximum Power

The maximum performances are evaluated at 6000 rpm considering the maximum phase current imposed for the initial requirements (500 A_{rms}). The results of the three proposed designs at maximum power are shown in Table 6. Under the same conditions, the transient behaviour from a thermal point of view is also evaluated, starting from an ambient temperature of 50 °Cl the hotspot temperatures for different designs in the thermal transient area at maximum power are represented in Figure 5.
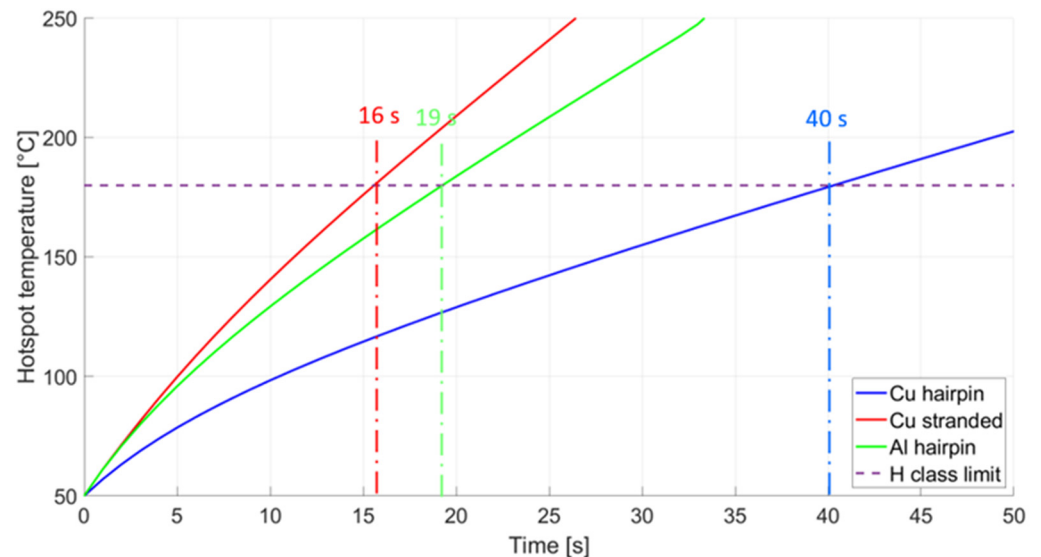
Figure 5. Hotspot temperatures in the thermal transient area at maximum power for the three proposed designs.

The three working points are chosen to work at maximum efficiency with the same current and speed. The most efficient project is D1 (89.53%), as expected, followed by D3 (−1.43%) and D2 (−3.33%)
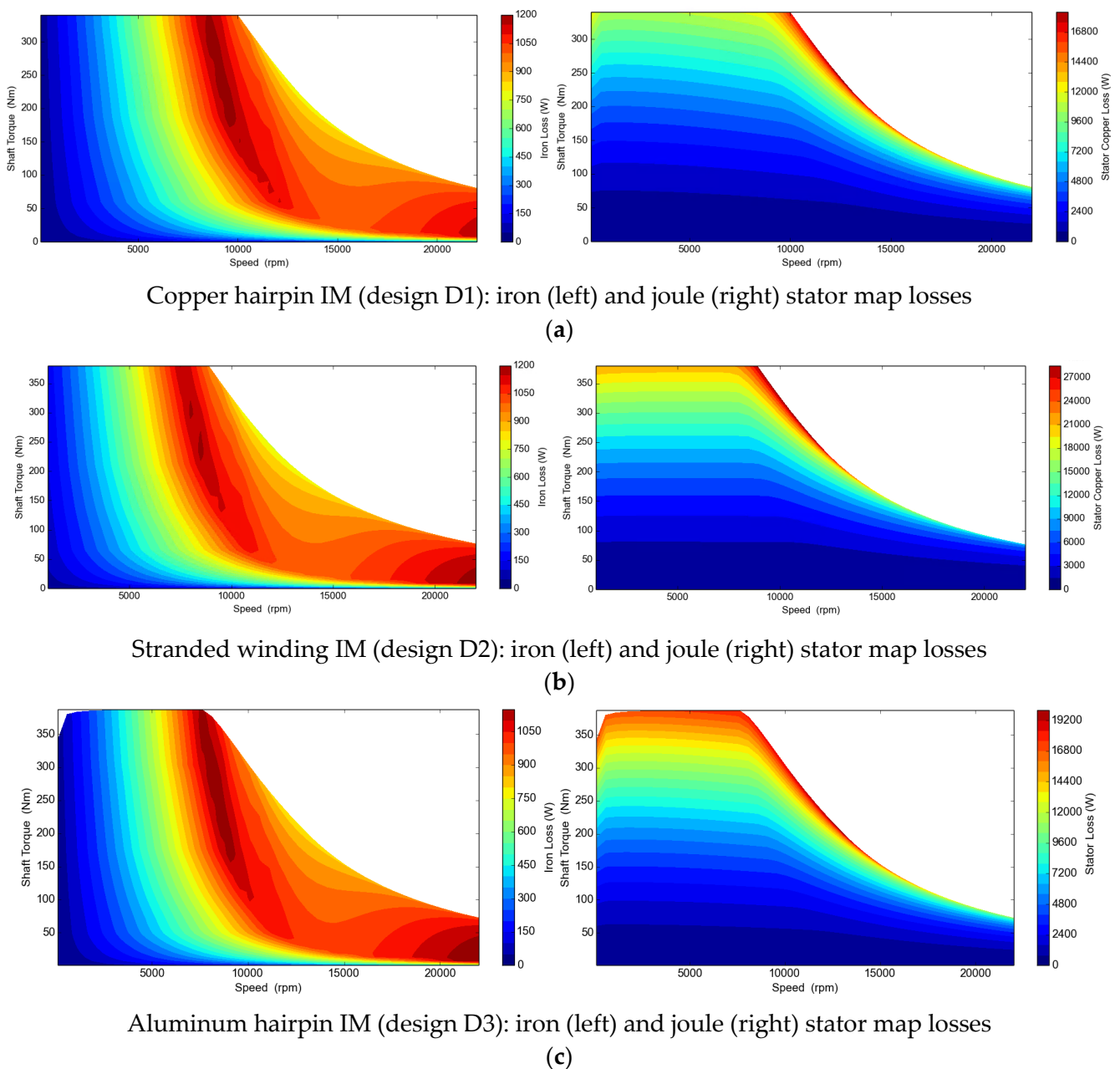
As expected, the initial design (D1) has a thermal transient at maximum power longer (40 s) than the other two solutions. Nevertheless, the higher efficiency of design D3 compared to D2 allows it to maintain the maximum current and higher torque and acceleration for a longer time (19 s respect to 16 s).

5. Efficiency and Losses Maps

The different loss contributions and the efficiency levels of the three designs are evaluated here in the operating range. The map is drawn considering the maximum torque per ampere control strategy (MTPA) and an appropriate field weakening strategy, where the voltage is a limitation up to a maximum speed of 22,000 rpm. The considered maximum current is the rated current (500 A_{rms}) and the DC bus voltage is 800 V with a maximum modulation index of 0.98 [35].

The following maps show the iron losses and stator winding losses, intending to show how relevant they are to the overall efficiency in an automotive context.
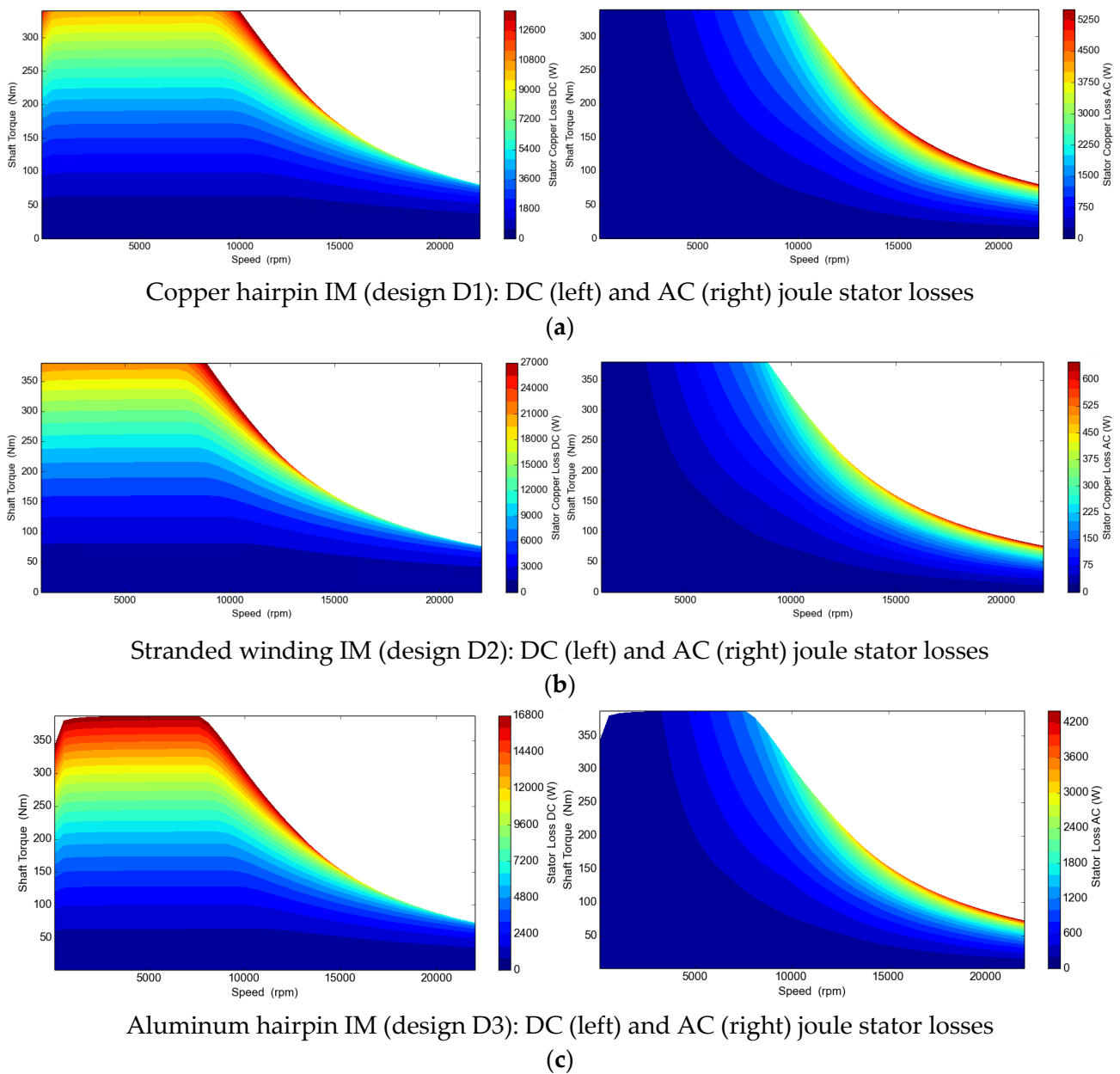
The total losses are strongly affected by the winding losses, as confirmed by the values reported in Figure 6. While the losses in the iron remain largely constant for the three cases, the joule losses in the windings strongly depend on the choice of winding technology used. In this regard, the losses in the stator windings are further explored and discussed in the maps in Figure 7, which detail DC and AC losses.

Copper hairpin IM (design D1): iron (left) and joule (right) stator map losses

(**a**)

Stranded winding IM (design D2): iron (left) and joule (right) stator map losses

(**b**)

Aluminum hairpin IM (design D3): iron (left) and joule (right) stator map losses

(**c**)

Figure 6. Maps of iron and joule stator losses for the three designs.

The analyses reported in Figure 7 show that the DC losses in the stator windings for D1 are lower than the other technologies, due to the low resistivity of copper and the large hairpin slot fill factor. On the other hand, and for the same reasons, the AC losses are larger than the other two projects. Despite this last consideration, the copper hairpins continue to be the choice that provide the lowest losses in the windings of the three designs. Design D2 allows for lower AC losses, even lower than design D3, but despite this the DC losses are significantly greater than the others. Design D3 is halfway between the other two in terms of the stator winding losses, both in terms of AC and DC losses.

In order to evaluate how these losses affect the motor efficiency, the efficiency maps are reported in Figure 8 for the operating torque and speed characteristics.

Copper hairpin IM (design D1): DC (left) and AC (right) joule stator losses

(**a**)

Stranded winding IM (design D2): DC (left) and AC (right) joule stator losses

(**b**)

Aluminum hairpin IM (design D3): DC (left) and AC (right) joule stator losses

(**c**)

Figure 7. Maps of DC and AC joule stator losses for the three considered designs.

The highest losses can be seen for the peak power operations (10–15 krpm), where the combined effect of the peak current, core saturation, and high frequency produces peak losses both in the windings and in the electrical steel material (Figure 8); nevertheless, the efficiency is maintained above 89% for all three cases in this speed range.

Furthermore, the efficiency maps confirm that design D3 has a trade-off between the performances of designs D1 and D2. In particular, the latter shows a reduction in the gap only at high speeds and high torques thanks to the lower AC losses. In detail, the point at maximum efficiency for D1 is 95.8%, for D2 it is 95.1% (−0.7%), and for D3 is 95.3% (−0.5%).
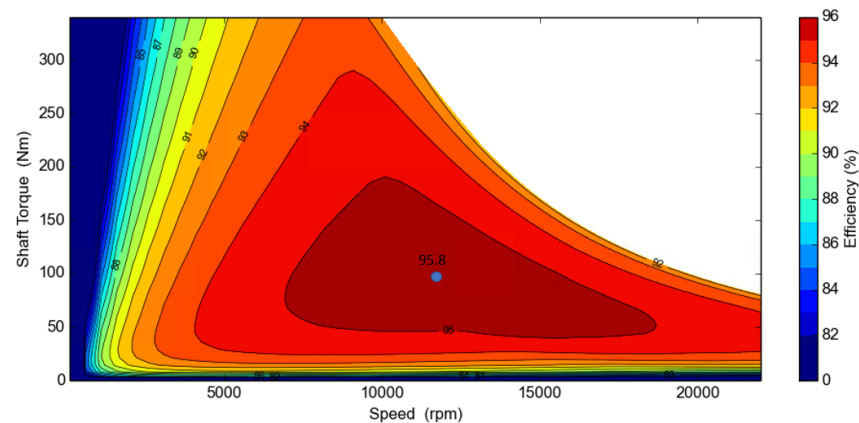
Copper hairpin IM (design D1): copper hairpin, efficiency

(**a**)
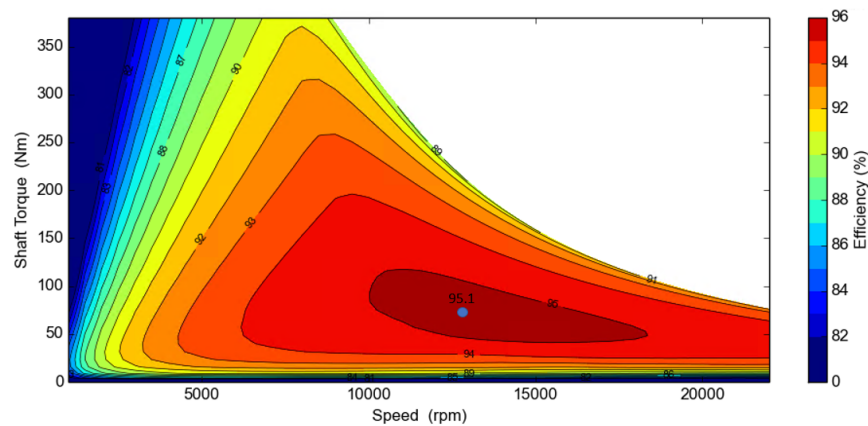
Stranded winding IM (design D2): stranded winding, efficiency

(**b**)
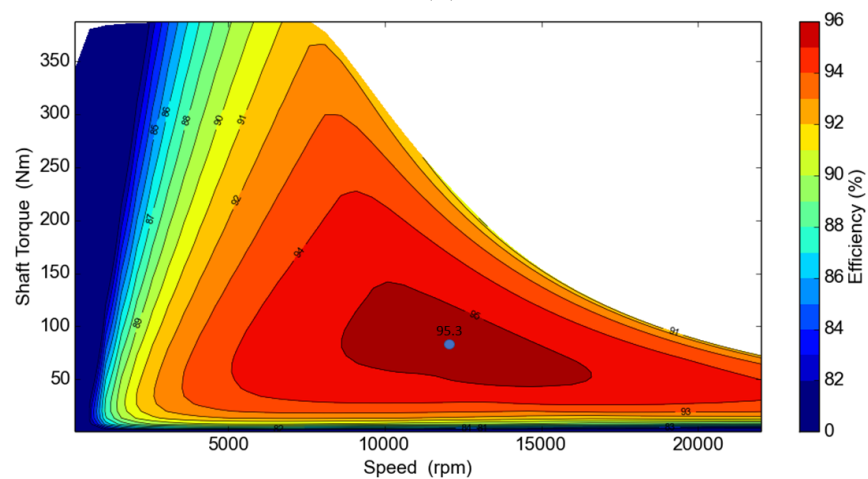
Aluminum hairpin IM (design D3): aluminum hairpin, efficiency

(**c**)

Figure 8. Efficiency maps for the three designs.

6. Performance on a Reference Drive Cycle

The aim of this section is to evaluate the performance of the three designs by considering a reference drive cycle and comparing the results for the different winding technologies. Indeed, in the driving cycle, the motor may operate with different torque and speed values, which for much of the time are even lower than the rated ones. The WLTP class 3 driving

cycle is selected to evaluate the performances of the three proposed designs, considering the target vehicle mass of 2500 kg, frontal area of 2.35 m^2, and gear ratio of 11.62 (wheel radius of 0.35 m). The torque, speed, and power required by the driving cycle are reported in Figure 9.
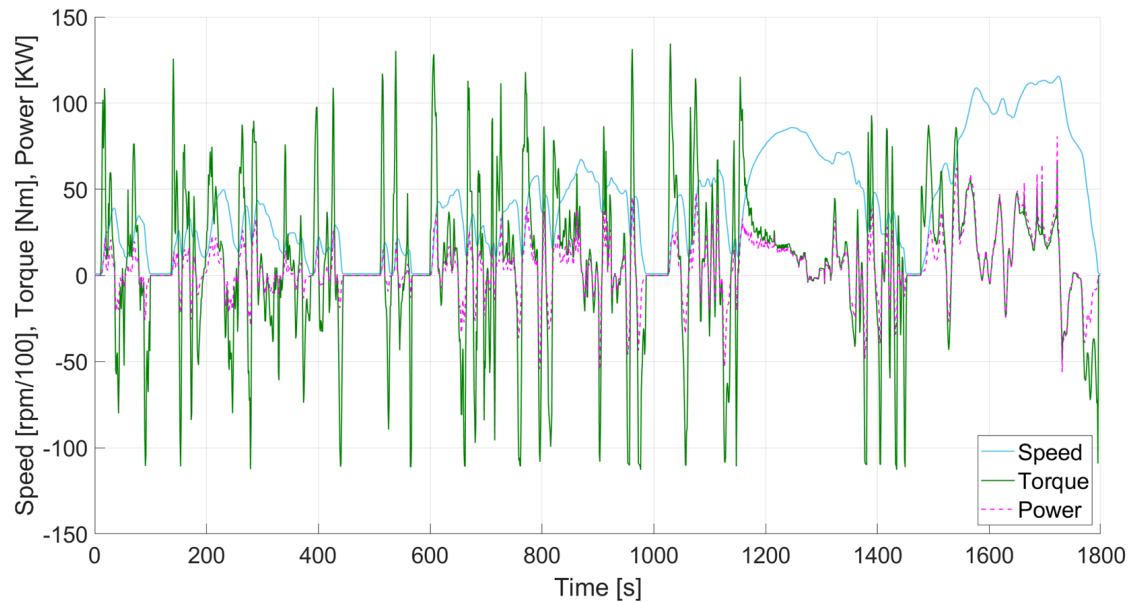

Figure 9. WLTP class 3 drive cycle: speed, shaft torque, and power vs. time.

The efficiency, RMS stator phase current, and RMS stator phase voltage are shown in Figures 10 and 11 for the different winding technologies.
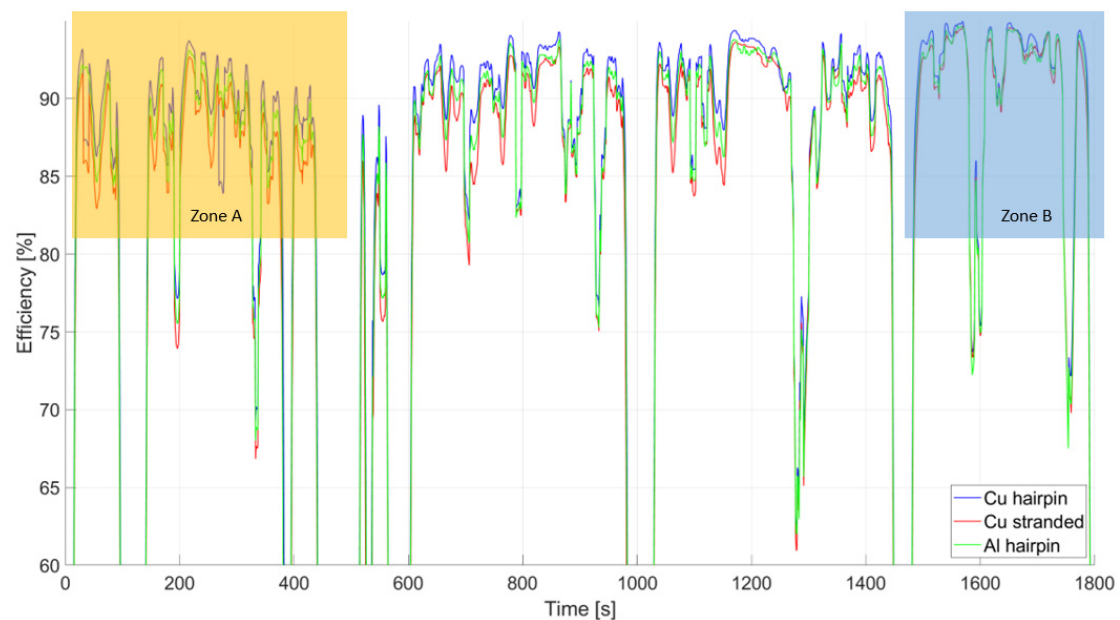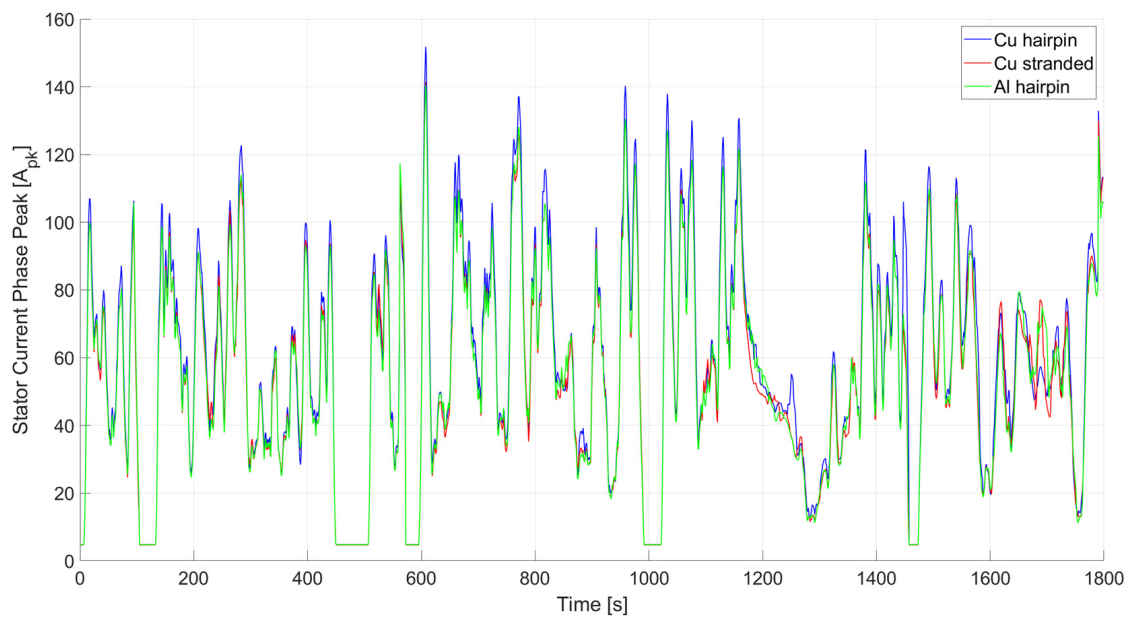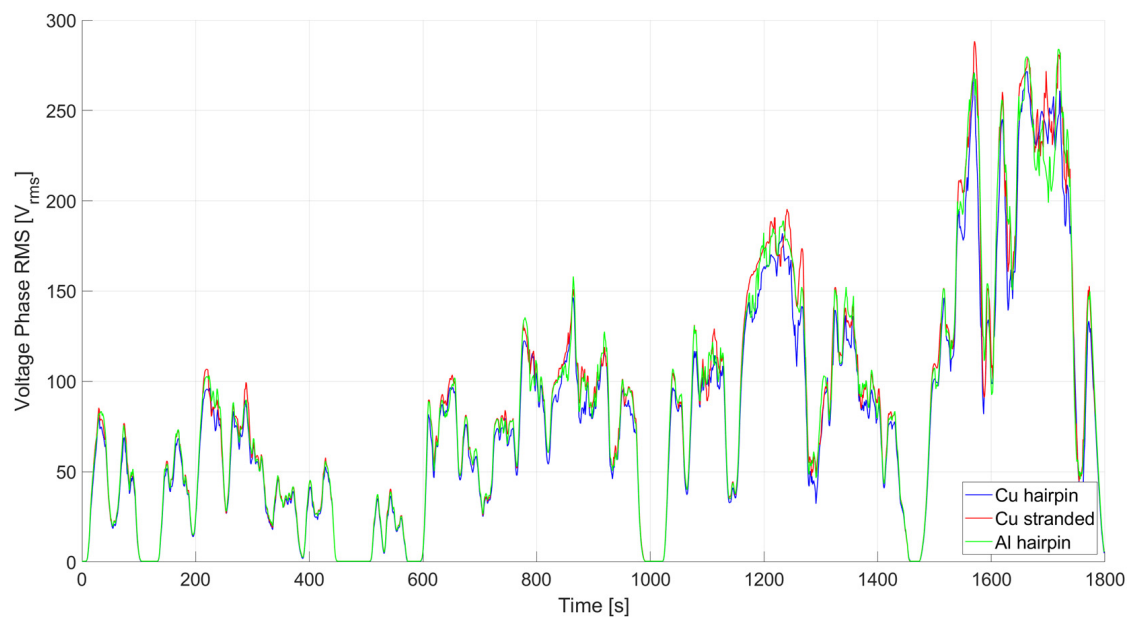

Figure 10. Efficiency in WLTP class 3 drive cycle.

RMS stator phase current over the WLTP 3 driving cycle

Figure 11. Efficiency, stator phase current (**top**), and voltage (**bottom**) values for WLTP class 3 drive cycle.

Concerning the efficiency in Figure 10, design D1 is always more efficient than the other two designs, despite the current required being higher (Figure 11). This is clearly closely related to the low resistance of D1 compared to D2 and D3. Moreover, the efficiency of D3 is, for most of the time, higher than D2, even though the required currents are quite similar.

In detail, two zones are highlighted in Figure 10 to focus on how the driving speed affects the efficiency. In zone A, where the speed required is lower, the differences between the efficiencies of the three projects are more evident, while at high speed this difference decreases. This is justified by looking at the previously reported efficiency maps, which in the higher speed zone are more similar than at low speeds.

Figure 11 shows how the voltage requirements of design D1 are practically always lower than in the other two designs.

The total losses in the stator windings are shown in Figure 12. In particular, to better investigate the joule losses, they are again detailed for DC and AC components.
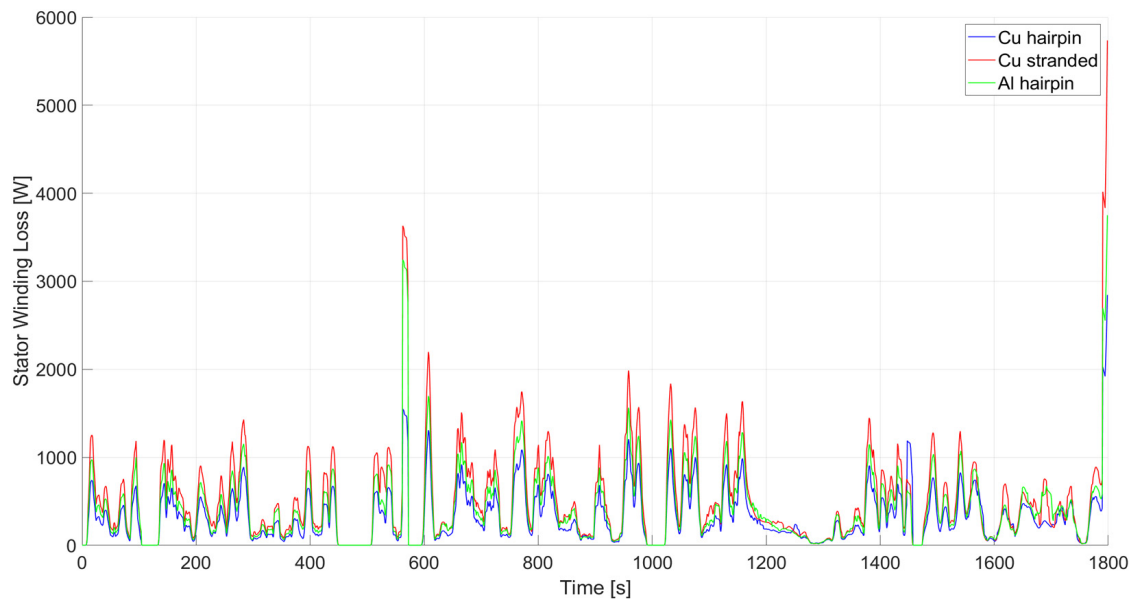
Stator joule losses over the WLTP 3 driving cycle
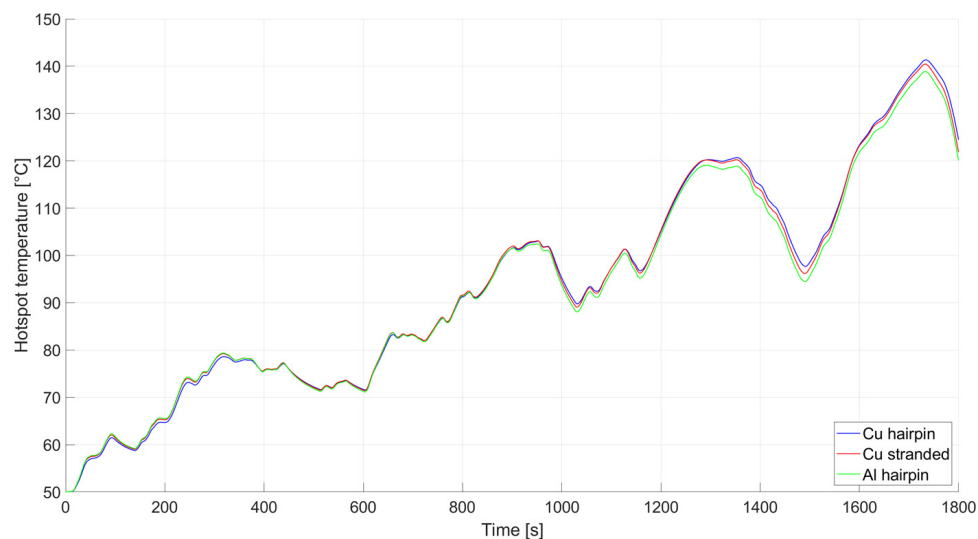
Figure 12. Stator winding losses in the WLTP class 3 drive cycle.

The results clearly show that AC losses, even in the worst case for copper hairpins, are considerably lower than DC losses. Hence, although the AC losses in the stranded windings are much lower than those in the hairpin bends, they do not represent the major component in joule losses. The same goes for the comparison between D1 and D3; even if the aluminium hairpins have lower AC losses, this does not make up for the disadvantage caused by the higher DC resistance with respect to the copper hairpins.

Figure 13 shows a comparison of the temperature trends for the motor hotspot over the entire drive cycle.

DC stator joule losses over the WLTP 3 driving cycle

AC stator joule losses over the WLTP 3 driving cycle
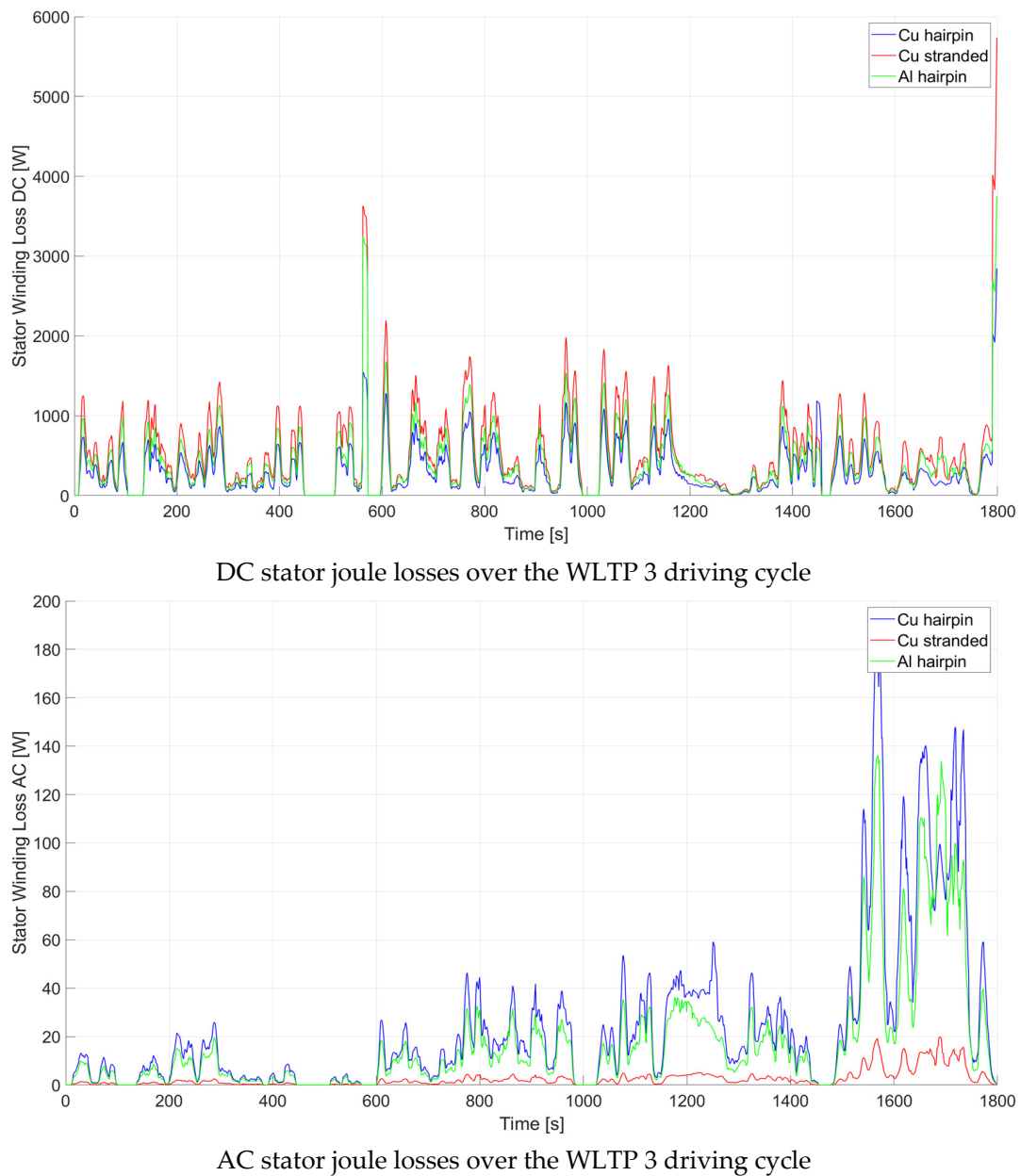
Figure 13. Hotspot temperatures in WLTP class 3 drive cycle.

In all three designs, the temperature is kept below the critical level for the considered insulation class. Concerning the hotspot temperature, it is interesting to note that D3 passes from an initial situation of a slight disadvantage to a slight advantage at the end of the drive cycle; this effect is due to the higher specific heat of aluminium compared to copper.

A comparative table of the results that emerged from the entire drive cycle is presented below (Table 7).

It can be noticed that the average energy efficiency is influenced in a relevant way by the winding technologies. As expected, design D1 has the best energy efficiency with a value of 93.05%, while the energy efficiency of design D3 is higher than that of design D2 (by about 1%). Indeed, the main differences among the three designs are related to the stator windings losses (D2 at +76% and D3 at +43% with respect to D1). The analyses on the WLTP driving cycle confirm the higher efficiency of the copper hairpin windings, while the aluminum hairpin windings seem to have efficiency benefits compared with stranded wires.

Table 7. Results for the WLTP class 3 drive cycle.

Description	D1	D2	D3
Energy Efficiency [1] (%)	93.05	91.01	91.76
Electric energy consumption (Wh)	3013	3151	3101
Electrical Input Energy (Wh)	4612	4714	4692
Shaft Motoring Energy (Wh)	4300	4300	4300
Electrical Output (Recovered) Energy (Wh)	1599	1563	1591
Shaft Generating Energy (Wh)	1728	1728	1728
Total Loss (Wh)	441	579	529
Stator Windings Loss (Wh)	147	261	211
Iron Loss (Wh)	83	104	101
Rotor Cage Loss (Wh)	44	47	49
Mechanical Loss (Wh)		52	
Motoring Operation (%)		70	
Generating Operation (%)		30	

[1] Defined as the ratio of the sum of the shaft motoring energy and the electrical output (Recovered) energy with respect to the sum of the electrical input energy and the shaft-generating energy.

7. Conclusions

This paper presents a detailed analysis of the performance of an induction motor for vehicle applications with different types of stator windings, namely copper hairpin, copper-stranded, and aluminum hairpin windings. After suitable adaptation of the three motors designs, they were evaluated both in terms of the rated operation and in peak power operation, including the thermal motor behavior.

From the analyses carried out here, the following general considerations can be outlined.

The copper hairpin winding technology (design D1) performs better from both an efficiency and thermal point of view. It exhibits peak performance over longer operating times, at more than twice the time length of the other technologies investigated. This is recommended in high-performance or premium vehicles, where peak operation and long-range efficiency is demanded. Nevertheless, the advantages are reduced in high-speed operations due to the AC copper losses, and special attention is needed for motors with more than 4 poles.

The copper-stranded round wire technology (design D2) is affected by the low slot fill factor, which increase the winding losses in the operating region of the machine. The rated and peak performance and the motor efficiency are affected by the higher winding losses, even if AC losses are contained in all the speed ranges of the motor. The adoption of this technology is recommended only for low-performance vehicles (mainly A-segment vehicles) with contained peak performance and limited range issues, unless a higher slot fill factor can be achieved using improved winding technologies.

A study of the suitability of the adoption of aluminum hairpins (design D3) for vehicle applications was the aim of the paper. The analysis carried out highlighted that this technology is a cost-effective approach that can guarantee a trade-off between copper hairpins and stranded wires at lower cost. Therefore, the aluminum hairpin technology is recommended in vehicle segments A to C, which require good torque densities and have heavy cost constraints. In those segments, the aluminum density and contained AC losses can allow for the development of high power density powertrains. Furthermore, the adoption of aluminum windings can reduce potential supply chain risks in mass production related to the high demand for copper windings in the growing renewable energy industry and electric vehicle market.

Moreover, the adoption of aluminum hairpins will improve the effectiveness in mass production scenarios, as the costs of the batteries are envisioned to decrease in the future and new battery technologies will be introduced to increase the vehicle range.

Further developments will address the adoption of aluminum winding technologies in early motor design stages and for different vehicles classes.

References

1. Nuzzo, S.; Barater, D.; Gerada, C.; Vai, P. Hairpin Windings: An Opportunity for Next-Generation E-Motors in Transportation. *IEEE Ind. Electron. Mag.* **2021**, 2–10. [CrossRef]
2. Ha, T.; Kim, D.K. Study of Injection Method for Maximizing Oil-Cooling Performance of Electric Vehicle Motor with Hairpin Winding. *Energies* **2021**, *14*, 747. [CrossRef]
3. Ha, T.; Han, N.G.; Kim, M.S.; Rho, K.H.; Kim, D.K. Experimental Study on Behavior of Coolants, Particularly the Oil-Cooling Method, in Electric Vehicle Motors Using Hairpin Winding. *Energies* **2021**, *14*, 956. [CrossRef]
4. Berardi, G.; Nategh, S.; Bianchi, N.; Thioliere, Y. A Comparison Between Random and Hairpin Winding in E-mobility Applications. In Proceedings of the IECON 2020 The 46th Annual Conference of the IEEE Industrial Electronics Society, Singapore, 19–21 October 2020; pp. 815–820. [CrossRef]
5. Mancinelli, P.; Stagnitta, S.; Cavallini, A. Lifetime analysis of an automotive electrical motor with hairpin wound stator. In Proceedings of the 2016 IEEE Conference on Electrical Insulation and Dielectric Phenomena (CEIDP), Toronto, ON, Canada, 16–19 October 2016; pp. 877–880. [CrossRef]
6. Raghuraman, B.; Nategh, S.; Sidiropoulos, N.; Petersson, L.; Boglietti, A. Sustainability Aspects of Electrical Machines For E-Mobility Applications Part I: A Design with Reduced Rare-earth Elements. In Proceedings of the IECON 2021 – 47th Annual Conference of the IEEE Industrial Electronics Society, Toronto, ON, Canada, 13–16 October 2021; pp. 1–6. [CrossRef]
7. Venturini, G.; Volpe, G.; Villani, M.; Popescu, M. Investigation of Cooling Solutions for Hairpin Winding in Traction Application. In Proceedings of the 2020 International Conference on Electrical Machines (ICEM), online, 23–26 August 2020; pp. 1573–1578. [CrossRef]
8. Venturini, G.; Volpe, G.; Popescu, M. Slot Water Jacket Cooling System for Traction Electrical Machines with Hairpin Windings: Analysis and Comparison. In Proceedings of the 2021 IEEE International Electric Machines & Drives Conference (IEMDC), Hartford, CT, USA, 17–20 May 2021; pp. 1–6. [CrossRef]
9. Gazdac, A.M.; di Leonardo, L.; Mabwe, A.M.; Betin, F.; Villani, M. Electric circuit parameters identification and control strategy of dual-rotor Permanent Magnet Induction Machine. In Proceedings of the 2013 International Electric Machines & Drives Conference, Chicago, IL, USA, 12–15 May 2013; pp. 1102–1107. [CrossRef]
10. Pastura, M.; Barater, D.; Nuzzo, S.; Franceschini, G. Multi Three-Phase Hairpin Windings for High-Speed Electrical Machine: Possible Implementations. In Proceedings of the 2021 IEEE Workshop on Electrical Machines Design, Control and Diagnosis (WEMDCD), Torino, Italy, 26–27 March 2021; pp. 113–118. [CrossRef]
11. Xue, S.; Michon, M.; Popescu, M.; Volpe, G. Optimisation of Hairpin Winding in Electric Traction Motor Applications. In Proceedings of the 2021 IEEE International Electric Machines & Drives Conference (IEMDC), Hartford, CT, USA, 17–20 May 2021; pp. 1–7. [CrossRef]
12. Ferkal, K.; Poloujadoff, M.; Dorison, E. Proximity effect and eddy current losses in insulated cables. *IEEE Trans. Power Deliv.* **1996**, *11*, 1171–1178. [CrossRef]
13. Du-Bar, C.; Wallmark, O. Eddy Current Losses in a Hairpin Winding for an Automotive Application. In Proceedings of the 2018 XIII International Conference on Electrical Machines (ICEM), Alexandroupoli, Greece, 3–6 September 2018; pp. 710–716.
14. Leonardo, L.D.; Popescu, M.; Villani, M. Eddy-Current Losses evaluation in hairpin wound motor fed by PWM Inverter. In Proceedings of the IECON 2020 The 46th Annual Conference of the IEEE Industrial Electronics Society, Singapore, 19–21 October 2020; pp. 943–948. [CrossRef]
15. di Leonardo, L.; Credo, A.; Tursini, M.; Villani, M. Rapid analytical method to evaluate eddy current losses in hairpin wound IM due to PWM. In Proceedings of the IECON 2021—47th Annual Conference of the IEEE Industrial Electronics Society, Toronto, ON, Canada, 13–16 October 2021; pp. 1–6. [CrossRef]
16. Zhu, S.; Paciura, K.; Barden, R. Design Approach of Hairpin Winding Motor with High Parallel Path Numbers. In Proceedings of the 2021 IEEE Energy Conversion Congress and Exposition (ECCE), Virtual, 10–14 October 2021; pp. 4534–4538. [CrossRef]
17. Arzillo, A.; Braglia, P.; Nuzzo, S.; Barater, D.; Franceschini, G.; Gerada, D.; Gerada, C. Challenges and Future opportunities of Hairpin Technologies. In Proceedings of the 2020 IEEE 29th International Symposium on Industrial Electronics (ISIE), Delft, The Netherlands, 17–19 June 2020; pp. 277–282. [CrossRef]

18. Glaessel, T.; Seefried, J.; Masuch, M.; Riedel, A.; Mayr, A.; Kuehl, A.; Franke, J. Process Reliable Laser Welding of Hairpin Windings for Automotive Traction Drives. In Proceedings of the 2019 International Conference on Engineering, Science, and Industrial Applications (ICESI), Tokyo, Japan, 22–24 August 2019; pp. 1–6. [CrossRef]

19. Glaessel, T.; Pinhal, D.B.; Masuch, M.; Gerling, D.; Franke, J. Manufacturing Influences on the Motor Performance of Traction Drives with Hairpin Winding. In Proceedings of the 2019 9th International Electric Drives Production Conference (EDPC), Esslingen, Germany, 3–4 December 2019; pp. 1–8. [CrossRef]

20. Halwas, M.; Blanc, F.S.-L.; Jux, B.; Doppelbauer, M.; Wirth, F.; Hausmann, L.; Hofmann, J.; Fleischer, J. Coherences Between Production Technology and Performance of Electric Traction Drives. In Proceedings of the 2019 9th International Electric Drives Production Conference (EDPC), Esslingen, Germany, 3–4 December 2019; pp. 1–9. [CrossRef]

21. Acquaviva, A.; Diana, M.; Raghuraman, B.; Petersson, L.; Nategh, S. Sustainability Aspects of Electrical Machines For E-Mobility Applications Part II: Aluminium Hairpin vs. Copper Hairpin. In Proceedings of the IECON 2021—47th Annual Conference of the IEEE Industrial Electronics Society, Toronto, ON, Canada, 13–16 October 2021; pp. 1–6. [CrossRef]

22. Dhulipati, H.; Mukundan, S.; Chauvin, L.; Riczu, C.; Edrisy, A.; Kozdras, M.; Bauman, J.; Habibi, S.; Tjong, J.; Kar, N.C. Investigation of Aluminium and Copper Wound PMSM for Direct–drive Electric Vehicle Application. *IOP Conf. Ser. Mater. Sci. Eng. (Online)* **2019**, *654*, 012002. [CrossRef]

23. Widmer, J.D.; Martin, R.; Mecrow, B.C. Precompressed and Stranded Aluminum Motor Windings for Traction Motors. *IEEE Trans. Ind. Appl.* **2016**, *52*, 2215–2223. [CrossRef]

24. Hafiz, K.; Nanda, G.; Kar, N.C. Comparative performance analysis of aluminum-rotor and copper-rotor SEIG considering skin effect. In Proceedings of the 2008 18th International Conference on Electrical Machines, Vilamoura, Portugal, 6–9 September 2008; pp. 1–6. [CrossRef]

25. Olivares-Galvan, J.C.; de León, F.; Georgilakis, P.S.; Escarela-Perez, R. Selection of Copper versus Aluminum Windings for Distribuztion Transformers. *IET Electr. Power Appl.* **2010**, *4*, 474–485.

26. Zainuddin, N.M.; Rahman, M.S.A.; Kadir, M.Z.A.A.; Ali, N.H.N.; Ali, Z.; Osman, M.; Mansor, M.; Ariffin, A.M.; Rahman, M.S.A.; Nor, S.F.M.; et al. Review of Thermal Stress and Condition Monitoring Technologies for Overhead Transmission Lines: Issues and Challenges. *Access IEEE* **2020**, *8*, 120053–120081. [CrossRef]

27. U.S. Geological Survey. Mineral Commodity Summaries, January 2022. Available online: https://pubs.usgs.gov/periodicals/mcs2022/mcs2022-copper.pdf (accessed on 1 May 2022).

28. Pastura, M.; Barater, D.; Nuzzo, S.; Franceschini, G. Investigation of Resistivity Impact on AC Losses in Hairpin Conductors. In Proceedings of the IECON 2021—47th Annual Conference of the IEEE Industrial Electronics Society, Toronto, ON, Canada, 13–16 October 2021; pp. 1–6. [CrossRef]

29. Choi, M.; Choi, G. Modeling, Investigation, and Mitigation of AC Losses in IPM Machines with Hairpin Windings for EV Applications. *Energies* **2021**, *14*, 8034. [CrossRef]

30. Glaessel, T.; Seefried, J.; Franke, J. Challenges in the manufacturing of hairpin windings and application opportunities of infrared lasers for the contacting process. In Proceedings of the 2017 7th International Electric Drives Production Conference (EDPC), Wuerzburg, Germany, 5–6 December 2017; pp. 1–7. [CrossRef]

31. Popescu, M.; Riviere, N.; Volpe, G.; Villani, M.; Fabri, G.; di Leonardo, L. A Copper Rotor Induction Motor Solution for Electrical Vehicles Traction System. In Proceedings of the 2019 IEEE Energy Conversion Congress and Exposition (ECCE), Baltimore, MD, USA, 29 September–3 October 2019; pp. 3924–3930. [CrossRef]

32. Refreedrive Official Website. Available online: www.refreedrive.eu (accessed on 1 May 2022).

33. di Leonardo, L.; Popescu, M.; Fabri, G.; Tursini, M. Performance Evaluation of an Induction Motor Drive for Traction Application. In Proceedings of the IECON 2019—45th Annual Conference of the IEEE Industrial Electronics Society, Lisbon, Portugal, 14–17 October 2019; pp. 4360–4365. [CrossRef]

34. Rivière, N.; Volpe, G.; Villani, M.; Fabri, G.; di Leonardo, L.; Popescu, M. Design Analysis of a High Speed Copper Rotor Induction Motor for a Traction Application. In Proceedings of the 2019 IEEE International Electric Machines & Drives Conference (IEMDC), San Deigo, CA, USA, 12–15 May 2019; pp. 1024–1031. [CrossRef]

35. di Leonardo, L.; Popescu, M.; Tursini, M.; Villani, M. Finite Elements Model Co-Simulation of an Induction Motor Drive for Traction Application. In Proceedings of the IECON 2019—45th Annual Conference of the IEEE Industrial Electronics Society, Lisbon, Portugal, 14–17 October 2019; pp. 1059–1065. [CrossRef]